Orientation and thickness dependence of magnetization at the interfaces of highly spin polarized manganite thin films

Rajesh V. Chopdekar,[1,2,*] Elke Arenholz,[3] and Yuri Suzuki[2]

[1]*School of Applied and Engineering Physics, Cornell University, Ithaca, NY 14853*

[2]*Department of Materials Science and Engineering, University of California, Berkeley, Berkeley, CA 94720*

[3]*Advanced Light Source, Lawrence Berkeley National Laboratory, Berkeley, CA 94720*

(Dated: January 14, 2009)

Abstract

We have probed the nature of magnetism at the surface of (001), (110) and (111)-oriented $La_{0.7}Sr_{0.3}MnO_3$ thin films. The spin polarization of $La_{0.7}Sr_{0.3}MnO_3$ thin films is not intrinsically suppressed at all surfaces and interfaces but is highly sensitive to both the epitaxial strain state as well as the substrate orientation. Through the use of soft x-ray spectroscopy, the magnetic properties of (001), (110) and (111)-oriented $La_{0.7}Sr_{0.3}MnO_3/SrTiO_3$ interfaces have been investigated and compared to bulk magnetometry and resistivity measurements. The magnetization of (110) and (111)-oriented $La_{0.7}Sr_{0.3}MnO_3/SrTiO_3$ interfaces are more bulk-like as a function of thickness whereas the magnetization at the (001)-oriented $La_{0.7}Sr_{0.3}MnO_3/SrTiO_3$ interface is suppressed significantly below a layer thickness of 20 nm. Such findings are correlated with the biaxial strain state of the $La_{0.7}Sr_{0.3}MnO_3$ films; for a given film thickness it is the tetragonal distortion of (001) $La_{0.7}Sr_{0.3}MnO_3$ that severely impacts the magnetization, whereas the trigonal distortion for (111)-oriented films and monoclinic distortion for (110)-oriented films have less of an impact. These observations provide evidence that surface magnetization and thus spin polarization depends strongly on the crystal surface orientation as well as epitaxial strain.

PACS numbers: 73.50.Jt, 75.47.Gk, 75.70.-i

I. INTRODUCTION

The nature of magnetism at surfaces and interfaces has been a fundamental issue that has yet to be completely understood. In particular, experiments probing the magnetization at the surface and interfaces of highly spin-polarized materials suggest that surface magnetization is suppressed compared to the bulk. These highly spin-polarized materials include complex transition metal oxides such as $La_{0.7}Sr_{0.3}MnO_3$ (LSMO) and Fe_3O_4. For example, Park *et al*. showed that in (001)-oriented LSMO thin films, surface magnetization, as measured by spin-polarized photoemission or soft x-ray spectroscopy, falls much more rapidly than bulk as a function of temperature.[1] More recently, Infante *et al*. have found that (110)-oriented $La_{0.7}Ca_{0.3}MnO_3$ (LCMO) thin films exhibit a slower decay of magnetization as a function of increasing temperature compared to (001)-oriented LCMO films.[2] Other spin polarized photoemission studies of Fe_3O_4 have reported spin polarization values ranging from -40 to -80% depending on the crystal surface being probed.[3–8] To date, the applicability of bulk spin polarization values at surfaces of highly spin polarized materials, such as LSMO or Fe_3O_4, and the dependence of these spin polarization values on crystal surface orientation has yet to be fully understood.

Given the potential of high spin polarization at LSMO surfaces,[9] many researchers have tried to use LSMO thin films in magnetic tunnel junctions but with mixed results. The figure of merit of magnetic tunnel junctions is tunneling magnetoresistance (TMR) which should be extremely high for devices with completely spin-polarized electrodes. To date, nearly half-metallic behavior has been observed in LSMO based junctions at low temperatures by a number of groups, but TMR falls quickly with increasing temperature.[10–12] TMR values in (001)-oriented Fe_3O_4 based junctions with $SrTiO_3$ or MgO barrier layers have exhibited TMR only at low temperatures.[13] More recently, the observation of large temperature dependent tunneling in Fe/MgO/Fe junctions and of significant TMR values in LSMO and Fe_3O_4 based magnetic tunnel junctions has prompted a reinvestigation of the nature of magnetism at the surfaces and interfaces of highly spin polarized materials.[14,15]

Correlating the structure and magnetism from multiple magnetic species at complex oxide heterointerfaces is crucial in understanding the nature of magnetism at surfaces and interfaces of highly spin polarized materials such as LSMO. Optimally doped LSMO has a rhombohedral perovskite structure where the magnetic order is found in octahedrally

coordinated Mn^{3+} and Mn^{4+} sites.[16] Element-specific and interface sensitive probes such as X-ray absorption spectroscopy (XAS) and X-ray magnetic circular dichroism (XMCD) have proven to be powerful tools to determine the details of interface magnetism since they allow for the determination of interface cation magnetization in an element, valence, and even site-sensitive manner.

In this paper, we present a study of the magnetism at the surfaces and interfaces of (001), (110) and (111)-oriented $La_{0.7}Sr_{0.3}MnO_3$. Detailed spectroscopy experiments indicate that magnetism at the (110) and (111)-oriented LSMO surface is not substantially reduced while at the (001)-oriented LSMO surface magnetism is significantly suppressed in agreement with previous spin polarized photoemission experiments.[1] Our results on LSMO surfaces and interfaces, combined with previous magnetization studies of (001) LSMO samples,[1,3] indicate that spin polarization is not intrinsically suppressed at the surface or interface but depends on the crystal surface orientation and reconstruction as well as epitaxial film strain.

II. EXPERIMENTAL

In order to probe the magnetization at $La_{0.7}Sr_{0.3}MnO_3$ surfaces and interfaces, we have synthesized epitaxial LSMO thin films by pulsed laser deposition on (001), (110) and (111)-oriented $SrTiO_3$ (STO) substrates supplied by Crystec GmbH. Two types of samples with uniform thickness were prepared: 5 nm single layers of LSMO and 50 nm LSMO layers with STO cap layers of 1-2 nm thickness. In addition, 10 mm x 5 mm 'wedge' samples were fabricated with a uniform STO cap layer and a LSMO film thickness ranging from 5-40 nm along the sample long axis to study thickness-dependent effects. Commercial sintered powder targets of stoichiometric single-phase oxides were used for ablation at an energy density of 1-1.5 J/cm^2. Deposition parameters for single layers are as follows: LSMO in 320 mTorr of O_2 at 700°C and $SrTiO_{3-\delta}$ in a 15 mTorr of O_2 at 600°C. Samples were cooled to room temperature at 10 K/min in a 300 Torr O_2 ambient.

Structural characterization of the thin films included atomic force microscopy in a Digital Instruments Dimension 3100 microscope to characterize the surface morphology of the deposited films. X-ray diffraction and reciprocal lattice mapping was performed on a Philips Analytical X'pert MRD diffractometer to study the crystallinity and strain state of the epitaxial layers. Film thickness for both uniform and wedge samples was determined by fitting

intensity oscillations around the Bragg peak to the Laue equation. As the beam size in the MRD can be of order 1 mm, the thickness variation across the wedge was confirmed from a 0.2 mm wide collimated beam at beamline 7.2 of the Stanford Synchrotron Radiation Laboratory.[17]

Field and temperature-dependent magnetization measurements for both single layers and magnetic layers with an STO cap were performed in a Lake Shore Cryotronics series 7300 Vibrating Sample Magnetometer as well as a Quantum Design MPMS 5XL magnetometer, and resistivity measurements were performed in a modified Quantum Design Physical Property Measurement System. The resistivity of films with uniform thickness were measured using the van der Pauw technique, while the wedge samples were sectioned into ten parts and resistivity was measured by a 4-point-in-line technique.

Soft x-ray absorption spectroscopy experiments in total electron yield (TEY) mode were performed at beamlines 4.0.2[18] and 6.3.1[19] of the Advanced Light Source (ALS) at Lawrence Berkeley National Laboratory. Spectroscopy experiments were performed with the sample surface normal 60° inclined from the x-ray beam from 25 K to 325 K in fields of up to 0.8 T. The x-ray beam height was approximately 0.2 mm; thus the quoted thickness for measurements on the wedge samples have an uncertainty in film thickness of 0.6 nm.

III. STRUCTURE

Surface morphology for LSMO single films and magnetic layers with STO caps on (001), (110) and (111)-oriented STO was smooth, with maximum RMS surface roughness for 50 nm thick films of 0.22 nm, 0.78 nm and 0.21 nm, respectively. In general, LSMO films had rougher morphology on (110)STO substrates as compared to (001) and (111)-oriented STO substrates. X-ray diffraction analysis reveals that LSMO films undergo different distortions from the rhombohedral unit cell depending on substrate orientation. In addition, reciprocal lattice maps of asymmetric reflections for the three orientations at the two extreme ends (5 nm and 35 nm film thickness) of the wedge samples are shown in Figure 1. Regardless of film thickness across the wedge, the film is pseudomorphically matched to the in-plane substrate lattice parameter as shown by the same q_x values for film and substrate reflections.

The type and extent of the distortion of the unit cell varies with substrate orientation. The rhombohedral unit cell undergoes a biaxial tensile stress on (001)-oriented STO that

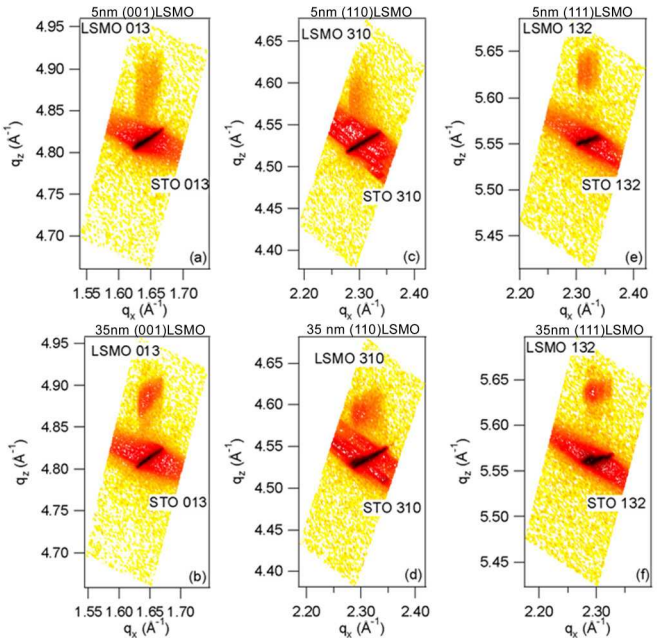

FIG. 1: (Color online) Reciprocal lattice maps for two different LSMO layer thicknesses of the LSMO/STO wedges as a function of orientation: (a) 5 nm LSMO(001), (b) 35 nm LSMO(001), (c) 5 nm LSMO(110), (d) 35 nm LSMO(110), (e) 5 nm LSMO(111), (f) 35 nm LSMO(111).

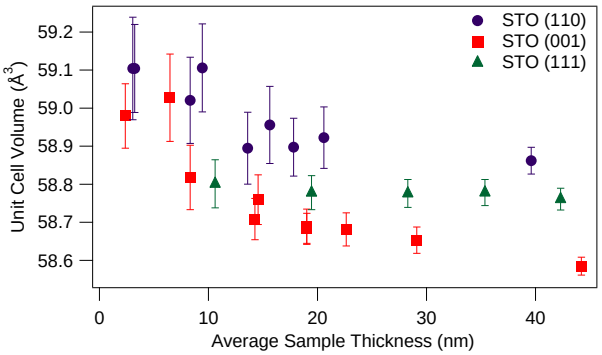

FIG. 2: (Color online) Unit cell volume determined from x-ray diffraction as a function of film orientation for both wedge-type samples as well as LSMO films of uniform thickness. Error bars indicate the full-width of the film reflection at half-maximum intensity. The unit cell volume bulk value for LSMO is 58.1 $\mathring{A}^3$.

imposes a tetragonal distortion on the unit cell. On the other hand, (110) and (111)-oriented STO impose a monoclinic and trigonal distortion of the unit cell, respectively. Thus even with the pseudomorphic nature of the films on all three orientations, we would expect the out of plane distortion to differ as a function of orientation due to the anisotropic Young's moduli

of LSMO films.[20] Calculation of the biaxial moduli[21] for LSMO films based on Darling *et al.*'s tabulated elastic constants on an $La_{0.83}Sr_{0.17}MnO_3$ single crystal[22] yields M_{001} = 164 GPa, M_{111} = 268 GPa, M_{110}^{001} = 211 GPa, and $M_{110}^{1\bar{1}0}$ = 279 GPa at T = 300 K. While the biaxial modulus is isotropic in the plane for (001) and (111)-oriented films, a large difference in modulus exists along the orthogonal in-plane directions for a (110) LSMO film. In spite of the variation in the magnitude of the biaxial modulus, none of the LSMO wedges relax to the bulk pseudocubic lattice parameter of 3.873 $\mathring{A}$,[23] and instead converge towards an out of plane value of 3.84-3.86 $\mathring{A}$ (Figure 2). The relaxed pseudocubic cell volume is approximately 58.1 $\mathring{A}^3$ and the distorted cell volume for the 35 nm thick end of the wedges is 1% larger. At small film thicknesses the unit cell volume is not preserved, and thus we would expect substantial changes in the magnetic behavior of the films for all three orientations due to out-of-plane or in-plane changes in the Mn-O-Mn bond angle and bond length.

IV. TRANSPORT

In colossal magnetoresistive manganites, the metal-insulator transition is coincident with the magnetic transition as described by the double exchange mechanism.[24] Thus, resistivity measurements may be performed to determine the onset and evolution of both ferromagnetism and metallicity in the LSMO films. Figures 3 (a)-(c) compare the field-dependent sheet resistivity of STO-capped 50 nm LSMO films, and the normalized ratio between resistivity in zero field and in an applied field out of the plane of the sample $MR(H,T) = (\rho(H,T) - \rho(0,T))/\rho(0,T)$ approaches -35% for all three samples at H = 5 T. The peak value in magnetoresistance (MR), T_{peak}, is used as an approximate measure of the Curie temperature T_c, and is plotted as a function of sample thickness in Figure 4. Below 8 nm the LSMO transition temperature drops substantially from the bulk value of 360 K for all samples. Above 8 nm, the (111)-oriented LSMO films have a constant transition temperature with thickness which is consistent with the unit cell volume data in Figure 2. On the other hand, the (110)-oriented LSMO film transition temperature increases with increasing film thickness without saturating at the largest film thickness on the wedge. Finally, the (001)LSMO films have the largest difference in out of plane lattice parameter compared to bulk, yet the transition temperature above a thickness of 8 nm is consistently larger than its (111)LSMO counterpart. While finite size effects and gradual loss of the ferromagnetic

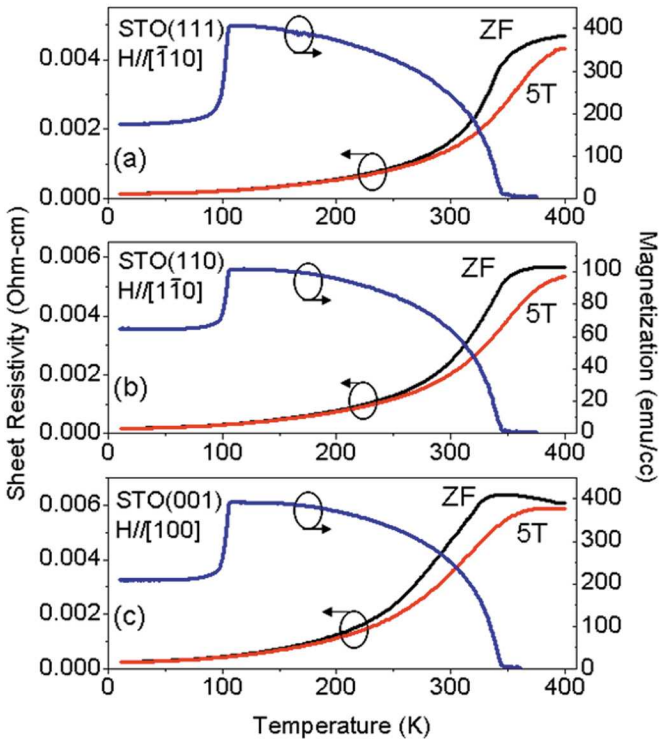

FIG. 3: (Color online) Sheet resistivity and magnetization of 2 nm STO/50 nm LSMO films on various orientations of STO. ZF and 5T refer to resistivity measurements taken in H = 0 T and H = 5 T with decreasing temperature. Magnetization was measured upon sample cooling in a field of 0.001 T.

metallic state below 8 nm dominate the transport behavior, above a film thickness of 8 nm crystal orientation plays a large role in determining the transport properties Such loss of ferromagnetism has also been seen in films of (001)-oriented LSMO below a thickness of 3-5 nm when grown on (001) $LaAlO_3$ and (110) $NdGaO_3$ substrates.[25]

V. MAGNETISM

As the transport properties differ between samples of the same thickness but different orientations, the magnetic properties of such films should also vary due to the double-exchange mechanism. The magnitude of the bulk saturation moment at low temperature for the LSMO $x = 0.3$ stoichiometry is 3.7 μ_B per Mn or 600 emu/cm^3. For comparison, we plot the magnetization as a function of temperature for 50 nm thick films on STO (111), STO(110), and STO(001) at H = 0.001 T in Figure 3 (a), (b) and (c), respectively. The

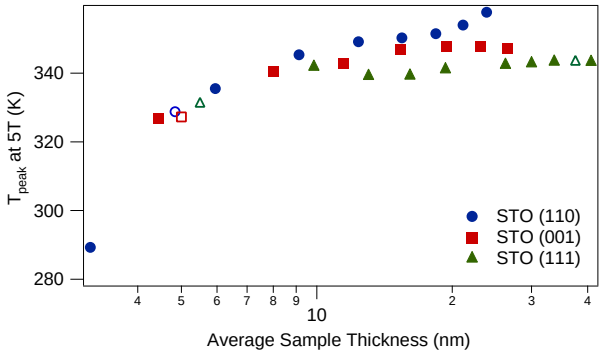

FIG. 4: (Color online) Temperature of the peak in magnetoresistance between zero field and H = 5 T as a function of LSMO film thickness. Open shapes are uniform films measured in the van der Pauw configuration, and solid shapes are measured in a 4-in-line contact configuration from 1mm sections of the wedge samples.

T_c obtained from the temperature-dependent magnetization data in 0.001 T matches well with the peak in MR. Saturation magnetization of 570-590 emu/cm^3, equivalent to 3.5-3.63 μ_B per Mn, is achieved at fields greater than 0.5 T at 10 K as shown in Figure 5 (a). The large two-fold in-plane anisotropy of (110)-oriented LSMO is inferred by the reduced low-field magnetization, but the saturation magnetization is consistent with the other film orientations.

The abrupt decrease in magnetization for all three types of samples in Figure 3 at 105 K is coincident with the STO cubic-tetragonal antiferrodistortive transition.[28] While the change in lattice parameter is on the order of 0.1%, the coherent strain state of the LSMO films is extremely sensitive to such breaking of symmetry as seen by the low-field magnetization data in Figures 5 (b) and (c). In thick manganite films on STO, strain relief occurs via creation of microtwin domains.[26,27] While the low field film anisotropy below the transition changes substantially as shown in Figure 5, this change is reversible and disappears for temperature-dependent magnetization scans taken at 3000 Oe. No coincident feature is observed in the zero-field resistivity, which suggests that there is no irreversible structural change in the films that would increase boundary scattering or other mechanism to alter transport properties. As near-bulk saturation magnetization can be obtained below this transition, this structural perturbation can be considered as a change in film anisotropy rather than a change in total film magnetization.

A quantitative analysis of the sample magnetization, composed of spin moment m_{spin} and

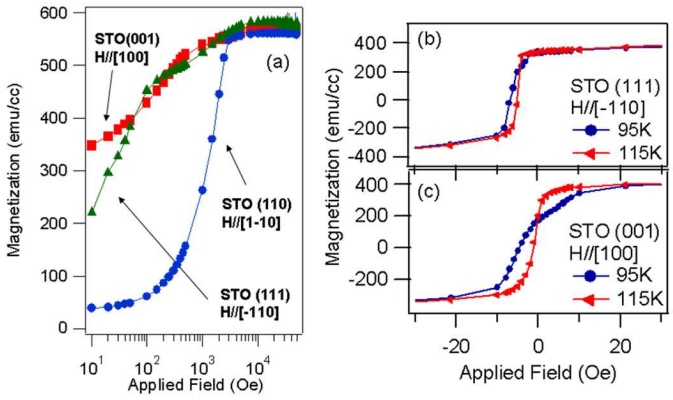

FIG. 5: (Color online) (a) Magnetization at T = 10 K with decreasing field for (001) (red squares), (110) (blue circles) and (111) (green triangles) -oriented LSMO films. All 3 samples saturate at approximately 580 emu/cc. Low-field magnetization for (b) (111)-oriented and (c) (001)-oriented films show marked differences above and below the structural transition of the STO substrate.

orbital moment m_{orb}, may be extracted from the experimental XMCD spectra through sum rule analysis for the $3d$ transition metals.[29,30] However, certain criteria must be met for sum rules to be applicable. For example, samples measured in grazing incidence invalidate the assumption that the total electron yield is proportional to the X-ray absorption coefficient due to electronic saturation effects.[31,32] In addition, for the lighter $3d$ transition metals, the comparatively small energy difference between the L_3 and L_2 absorption edges can lead to jj mixing and the transfer of spectral weight between the L_3 and L_2 absorption peaks.[33] Finally, a correction to the spin moment m_{spin} due to magnetic anisotropy from spin-orbit interactions and low-symmetry crystal field effects may not be negligible when calculating the spin moment for magnetic ions in non-cubic symmetry such as at surfaces and interfaces.[34] The correction may be represented by the expectation value of the magnetic dipole operator term $\langle T_z \rangle$. With this in mind, we analyze the relative change in extracted spin moment as a function of position across the wedge samples, and thus as a function of probe depth into the LSMO layer.

We can evaluate the spin moment $(m_{spin} + 7\langle T_z \rangle)$ and orbital moment m_{orb} using only the integrated intensity of the XAS and XMCD experimental spectra as well as the number of $3d$ electrons per transition metal cation. However, $7\langle T_z \rangle$ must be known to calculate m_{spin}. The evaluation of the spin moment may be performed as $m_s^* = (m_{spin} + 7\langle T_z \rangle) = (10 - N_{3d}) * (4q - 6p)/r$ where p is the XMCD integral over the L_3 edge, q is the XMCD integral over

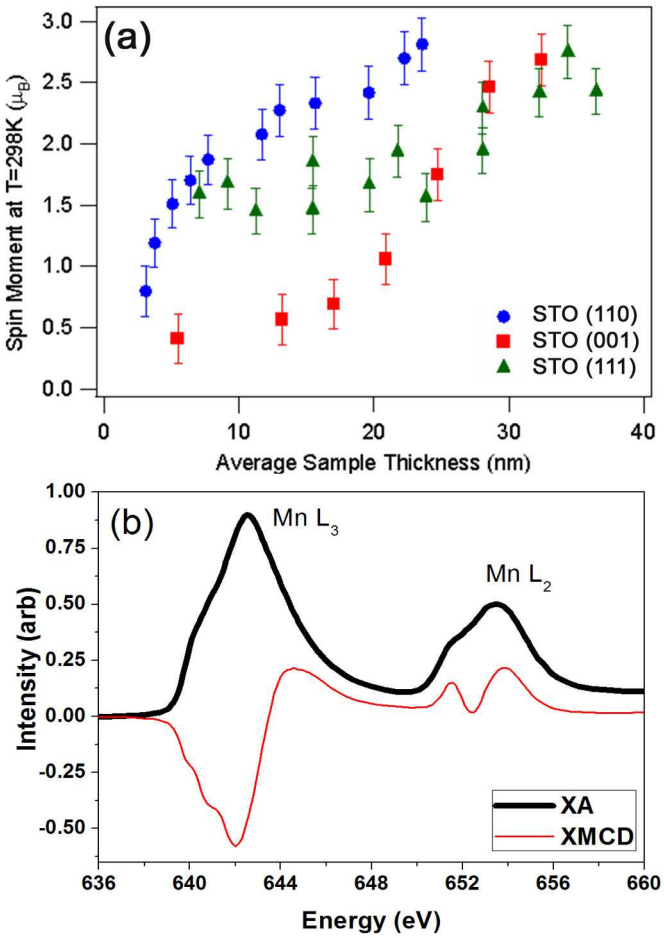

FIG. 6: (Color online) (a) Room temperature uncorrected spin moment m_s^* derived from XMCD spectra using sum rule analysis for LSMO films of various orientations as a function of thickness as compared to the expected value of 2.9 μ_B from room temperature magnetization measurements. The magnetic field of 1500 Oe was applied along the [100] direction for (001)LSMO, [001] for (110)LSMO, and [$\bar{1}$10] for (111)LSMO. (b) Absorption (black) and dichroism (red) lineshapes for the 28 nm section of the (001)LSMO wedge measured at room temperature.

both L_3 and L_2 edges, r is the XAS integral over L_3 and L_2 edges with the continuum background subtracted, and N_{3d} is the number of $3d$ electrons per cation. Without correction for magnetic anisotropy induced from spin orbit interactions or surface effects as represented by $\langle T_z \rangle$, m_s^* at the thickest portion of all three orientations of wedge layers is approximately 2.75 μ_B per Mn at room temperature at 1500 Oe.

Figure 6 (a) shows the room temperature uncorrected spin moment m_s^* measured at different positions on LSMO wedge/2 nm STO cap samples as a function of position along

the sample and thus as a function of LSMO film thickness for each orientation. In addition, Figure 6 (b) plots typical room-temperature x-ray absorption and dichroism spectra for the Mn $L_{3,2}$ edges of the LSMO samples with dichroism scaling corrections for X-ray circular polarization and angle of incidence with respect to the surface normal. A saturation magnetic field of 1500 Oe was applied along the [100] direction for (001)LSMO, [001] for (110)LSMO, and $[\bar{1}10]$ for (111)LSMO. While large fields are necessary to saturate the films at 10 K as shown in Figure 5 (a), 1500 Oe is enough to saturate all three samples at room temperature at 2.9 μ_B as verified by SQUID magnetometry. While the XMCD-derived spin moment of all three orientations converge towards a maximum value of 2.75 μ_B, it is the (110)LSMO film orientation that approaches the maximum value at the smallest film thicknesses. Park *et al.* had observed significant suppression of the magnetization at the surface of (001)-oriented 190 nm thick LSMO thin films,[1] and such a suppression is consistent with the reduction in spin moment of films up to 25 nm thick. Infante *et al.*'s more recent results,[2] indicating a difference in temperature dependence and Curie temperature of (001) and (110) LCMO thin films, are consistent with the recovery of the spin moment for our (110) and (111)-oriented LSMO films at smaller film thickness as compared to (001)LSMO films.

The dependence of spin polarization on the crystallographic orientation of LSMO suggests that the mere presence of a surface or interface does not necessarily suppress the spin polarization in these materials. Here A = $La_{0.7}Sr_{0.3}$ and B = Mn where ABO_3 is the perovskite structure. Experimentally, the (110) $[ABO]^{4+}$ surface of the perovskite appears to be more bulk-like magnetically compared to the $[AO]^{0.7+}$ or $[BO_2]^{0.7-}$ planes of the (001) surface. This difference stems in part due to the strong driving force to relieve strain that in turn affects the B-O-B exchange interaction.[35] Lebedev *et al.* found that microtwinning of the $La_{0.84}Sr_{0.16}MnO_3$ film on a (110)STO substrate occurred due to corrugation of the nominal (110) surface into (001) planes, thus allowing for strain relaxation without the need for the formation of interfacial misfit disloations.[36] It should be noted that the (001) ABO_3 cubic perovskite stacks with alternating $[AO]^{0.7+}$ and $[BO_2]^{0.7-}$ layers while the (110) orientation stacks with alternating $[ABO]^{4+}$ or $[O_2]^{4-}$ planes of atoms,[37,38] and the (111) orientation stacks with alternating $[AO_3]^{3.3-}$ and $[B]^{3.3+}$ planes.[39] The more polar (110) and (111) surfaces may be more susceptible to reconstruction and hence strain relaxation, thus allowing for the quicker recovery of spin moment as a function of film thickness.

A further examination of the room-temperature Mn L_3 XAS in Figure 7 illustrates that

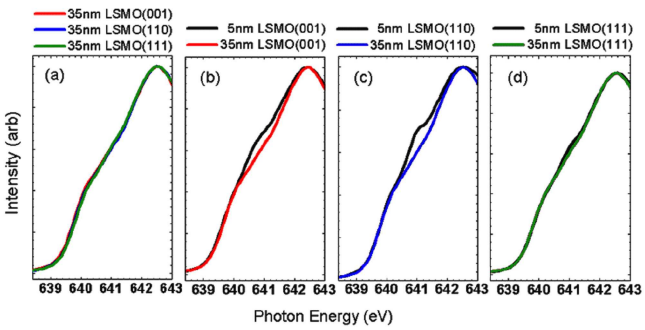

FIG. 7: (Color online) Mn L_3 x-ray absorption spectra as a function of film orientation. While the lineshapes for the 35 nm thick films (a) lie on top of each other, there is substantial difference in the lineshape for the (b) (001) and (c) (110)-oriented 5 nm LSMO films. In comparison, the (111)-oriented sample (d) shows little change in lineshape as a function of thickness.

35 nm films of all orientations exhibit identical lineshapes which implies that the same chemical environment exists at the interface of the LSMO film and STO cap layer. As film thickness is decreased below 35 nm, the Mn L_3 lineshape changes substantially for both (001) and (110) film orientations. de Jong *et al.* attribute a feature on the low photon energy side of the Mn L_3 absorption edge as originating from Mn^{2+},[40] but the suppression of magnetization for (001) films and retention of magnetization for (110) films point to the changing symmetry of the Mn environment under epitaxial strain as the cause of this change in Mn L_3 spectral weight. The weak thickness dependence of the (111)LSMO multiplet features can be correlated with the weak thickness dependence of both the lattice parameter as seen in Figure 2 as well as the spin moment as shown in Figure 6.

The difference in the unit cell volume for thin films of different orientations combined with the above change in spectral weight for the Mn L_3 lineshapes suggest that the Mn environment varies both as a function of strain and film orientation. Examination of strained (La,Ca)MnO_3 films illustrated that Mn-Mn cation distances and thus Mn-O bond angles varied under epitaxial strain.[41] A change in Mn-O bond angle results in variation of the double exchange transfer integral and thus directly affects both transport and magnetization properties. Clearly, the changes in structural symmetry due to epitaxial strain give rise to significant variations in surface spin polarization in LSMO, with the larger strain in thinner films resulting in substantial differences in spin moment at the surface. This variation can, in turn, be exploited by choosing (110) and (111)-oriented films that achieve near-bulk

magnetization for devices such as magnetic tunnel junctions in which the interface spin polarization plays a dominant role in determining device properties.

VI. CONCLUSION

In summary, we have found that the magnetization of (110) and (111)-oriented $La_{0.7}Sr_{0.3}MnO_3/SrTiO_3$ interfaces are more bulk-like as a function of thickness whereas the magnetization at the (001)-oriented $La_{0.7}Sr_{0.3}MnO_3/SrTiO_3$ interface is suppressed significantly below a layer thickness of 20 nm. Both magnetization and spin polarization depends on the crystal surface plane and is not equally suppressed for all surfaces or interfaces.

Acknowledgments

This research and the Advanced Light Source are supported by the Office of Basic Energy Sciences, Division of Materials Sciences and Engineering, of the U.S. Department of Energy under Contract No. DE-AC02-05CH11231. Portions of this research were carried out at the Stanford Synchrotron Radiation Laboratory (SSRL), a national user facility operated by Stanford University on behalf of the U.S. Department of Energy, Office of Basic Energy Sciences. RVC thanks Dr. Michael F. Toney (SSRL) and Brittany Nelson-Cheeseman for their assistance in verifying film thickness using hard X-ray scattering measurements.

---

* Electronic address: rvc2@cornell.edu

[1] J. H. Park, E. Vescovo, H. J. Kim, C. Kwon, R. Ramesh, and T. Venkatesan, Physical Review Letters **81**, 1953 (1998).

[2] I. C. Infante, F. Sanchez, J. Fontcuberta, S. Fusil, K. Bouzehouane, G. Herranz, A. Barthelemy, S. Estrade, J. Arbiol, F. Peiro, et al., Journal of Applied Physics **101**, 093902 (2007).

[3] D. J. Huang, C. F. Chang, J. Chen, L. H. Tjeng, A. D. Rata, W. P. Wu, S. C. Chung, H. J. Lin, T. Hibma, and C. T. Chen, Journal of Magnetism and Magnetic Materials **239**, 261 (2002).

[4] S. A. Morton, G. D. Waddill, S. Kim, I. K. Schuller, S. A. Chambers, and J. G. Tobin, Surface Science **513**, L451 (2002).

[5] M. Fonin, S. D. Yu, R. Pentcheva, R. U, and G. G, Journal of Physics: Condensed Matter **31**, 315217 (2007).

[6] E. Vescovo, H-J. Kim, J. M. Ablett, and S. A. Chambers, Journal of Applied Physics **98**, 084507 (2005).

[7] Y. S. Dedkov, U. Rudiger, and G. Guntherodt, Physical Review B **65**, 064417 (2002).

[8] J. G. Tobin, S. A. Morton, S. W. Yu, G. D. Waddill, I. K. Schuller, and S. A. Chambers, Journal of Physics: Condensed Matter **31**, 315218 (2007).

[9] H. Y. Hwang, S-W. Cheong, N. P. Ong, and B. Batlogg, Physical Review Letters **77**, 2041 (1996).

[10] Y. Lu, X. W. Li, G. Q. Gong, G. Xiao, A. Gupta, P. Lecoeur, J. Z. Sun, Y. Y. Wang, and V. P. Dravid, Physical Review B **54**, R8357 (1996).

[11] M. Viret, M. Drouet, J. Nassar, J. P. Contour, C. Fermon, and A. Fert, Europhysics Letters **39**, 545 (1997).

[12] M. Bowen, M. Bibes, A. Barthelemy, J. P. Contour, A. Anane, Y. Lemaitre, and A. Fert, Applied Physics Letters **82**, 233 (2003).

[13] S. B. Ogale, K. Ghosh, S. P. Pai, M. Robson, E. Li, I. Jin, R. L. Greene, R. Ramesh, T. Venkatesan, and M. Johnson, Materials Science and Engineering: B **56**, 134 (1998).

[14] S. S. P. Parkin, C. Kaiser, A. Panchula, P. M. Rice, B. Hughes, M. Samant, and S.-H. Yang, Nat Mater **3**, 862 (2004).

[15] W. H. Butler, X. G. Zhang, T. C. Schulthess, and J. M. MacLaren, Physical Review B, **63** 054416, (2001).

[16] P. G. Radaelli, M. Marezio, H. Y. Hwang, S. W. Cheong, and B. Batlogg, Physical Review B **54**, 8992 (1996).

[17] R. V. Chopdekar, B. B. Nelson-Cheeseman, M. F. Toney, and Y. Suzuki, unpublished data.

[18] A. T. Young, J. Feng, E. Arenholz, H. A. Padmore, T. Henderson, S. Marks, E. Hoyer, R. Schlueter, J. B. Kortright, V. Martynov, et al., Nuclear Instruments and Methods in Physics Research Section a-Accelerators Spectrometers Detectors and Associated Equipment **467**, 549 (2001).

[19] P. Nachimuthu, J. H. Underwood, C. D. Kemp, E. M. Gullikson, D. W. Lindle, D. K. Shuh, and R. C. C. Perera, in *Eighth International Conference on Synchrotron Radiation Instrumentation. San Francisco, CA* (2004).

[20] L. M. Berndt, V. Balbarin, and Y. Suzuki, Applied Physics Letters **77**, 2903 (2000).

[21] W. Nix, Metallurgical and Materials Transactions A **20**, 2217 (1989).

[22] T. W. Darling, A. Migliori, E. G. Moshopoulou, S. A. Trugman, J. J. Neumeier, J. L. Sarrao, A. R. Bishop, and J. D. Thompson, Physical Review B **57**, 5093 (1998).

[23] J. L. Maurice, F. Pailloux, A. Barthlmy, O. Durand, D. Imhoff, R. Lyonnet, A. Rocher, and J. P. Contour, Philosophical Magazine **83**, 3201 (2003).

[24] J. M. D. Coey, M. Viret, and S. von Molnar, Advances in Physics **48**, 167 (1999).

[25] J. Z. Sun, D. W. Abraham, R. A. Rao, and C. B. Eom, Applied Physics Letters **74**, 3017 (1999).

[26] F. Pailloux, R. Lyonnet, J.-L. Maurice, and J.-P. Contour, Applied Surface Science **177**, 263 (2001).

[27] M. Zhang, X. L. Ma, D. X. Li, H. B. Lu, Z. H. Chen, and G. Z. Yang, physica status solidi a **196**, 365 (2003).

[28] J. C. Slonczewski, and H. Thomas, Physical Review B **1**, 3599 (1970).

[29] C. T. Chen, Y. U. Idzerda, H. J. Lin, N. V. Smith, G. Meigs, E. Chaban, G. H. Ho, E. Pellegrin, and F. Sette, Physical Review Letters **75**, 152 (1995).

[30] B. T. Thole, P. Carra, F. Sette, and G. van der Laan, Physical Review Letters **68**, 1943 (1992).

[31] R. Nakajima, J. Stohr, and Y. U. Idzerda, Physical Review B **59**, 6421 (1999).

[32] S. Gota, M. Gautier-Soyer, and M. Sacchi, Physical Review B **62**, 4187 (2000).

[33] E. Goering, Philosophical Magazine **85**, 2895 (2005).

[34] R. Wu and A. J. Freeman, Physical Review Letters **73**, 1994 (1994).

[35] J. Fontcuberta, I. C. Infante, V. Laukhin, F. Sanchez, M. Wojcik, and E. Jedryka (AIP, 2006), vol. 99, p. 08A701.

[36] O. I. Lebedev, J. Verbeeck, G. Van Tendeloo, S. Amelinckx, F. S. Razavi, and H. U. Habermeier, Philosophical Magazine A **81**, 2865 (2001).

[37] E. Heifets, W. A. Goddard, E. A. Kotomin, R. I. Eglitis, and G. Borstel, Physical Review B **69**, 035408 (2004).

[38] Y. Mukunoki, N. Nakagawa, T. Susaki, and H. Y. Hwang, Applied Physics Letters **86**, 171908 (2005).

[39] A. Pojani, F. Finocchi, and C. Noguera, Surface Science **442**, 179 (1999).

[40] M. P. de Jong, I. Bergenti, V. A. Dediu, M. Fahlman, M. Marsi, and C. Taliani, Physical Review B **71**, 014434 (2005).

[41] A. Miniotas, A. Vailionis, E. B. Svedberg, and U. O. Karlsson, Journal of Applied Physics **89**, 2134 (2001).